

## EFFECTIVENESS OF ALUMINA DISPERSOIDS PARTICLES WITHIN (7XXX SERIES) ALUMINUM ALLOY UNDER THE RETROGRESSION AND REAGING TREATMENTS

HAIDER T. NAEEM\*

*School of Materials Engineering, University Malaysia Perlis, Jejawi, Perlis, Malaysia*

In this study, the effects of Alumina particles on the microstructure and the hardness of experimental an Al-Zn-Mg-Cu-Fe-Cr-Ni aluminum alloy matrix was produced using powder metallurgy. Aluminum matrix composite reinforced with Alumina ( $\text{Al}_2\text{O}_3$ ) particles of volume fraction 5% and average size about  $4\mu\text{m}$  was investigated. The prepared composite powders were consolidated by cold pressing and after that the sintered. The sintered composite samples have been subjected to a homogenizing condition then aged at (T6 temper) and retrogressed, and then re-aged (RRA). The results indicated that T6 heat treatment increases the hardness of an Al-composite compared to be as sintered. With applying the retrogression and reaging process, aluminum matrix composite has the highest hardness. These improvements attributed to the precipitation hardening of alloying elements besides, the dispersion strengthening of alumina particles and Ni-dispersoid intermetallic compound in the matrix. Microstructure characterization of an Aluminum matrix composite was carried out using optical microscopy (OM), scanning electron microscopy (SEM), energy dispersive spectroscopy (EDS) and X-ray diffraction (XRD).

(Received January 7, 2014; Accepted February 19, 2014)

*Keywords:* Al-Zn-Mg-Cu matrix composite;  $\text{Al}_2\text{O}_3$  particles; Aging treatment.

### 1. Introduction

Aluminum–alumina particle composites (AMCs) have great technological interests used in aviation, transportation, military industries and so forth, because of their properties such as the high ratio of strength/density, high specific modulus, a low coefficient thermal expansion and good electrical and thermal conductivity [1-3]. Widely studies have been carried out on Aluminum matrix composites to improve their mechanical and tribological properties because of the potential for weight is saving and service life increasing in many applications. Previous literatures indicated to use different ceramic particles as reinforcing materials within Aluminum PM Alloys such as  $\text{Al}_2\text{O}_3$  [4],  $\text{SiC}_p$  [5],  $\text{MgO}$  [6]. Between these aluminum alloys, the 7xxx series refers to a high response to compaction and sintering process addition to development of properties using ceramic particles [7, 8]. During the past decade, there have been some realizations on the influence heat treatment on mechanical properties of the AMCs that their matrixes are heat treatable aluminum alloys [9, 10, and 11] thus based to some of the outcomes; it is possible to improve the mechanical properties of such an AMCs with the aging.

In the present work, attempting made to produce alloy similar to the 7075 aluminum alloy matrix composite containing nickel additives addition to alumina ceramic particle using powder metallurgy technique. The aim is to study the effects of  $\text{Al}_2\text{O}_3$  particles on the microstructural and the hardness of composites under applying the retrogression and reaging heat treatments.

---

\*Corresponding author: haider\_neem@yahoo.com

## 2. Experimental Work

### 2.1 Materials

The P/M alloy studied for this work of the term (alloy A) has a nominal composition of Al-5.5Zn-2.5Mg-1.5Cu-0.4Fe-0.2Cr-1Ni-5Al<sub>2</sub>O<sub>3</sub> (all compositions in wt. pct.) were compacted from premixed, characteristics of the elemental powders as shown in Table 1; Particle size distribution was measured by Malvern Mastersizer 2000 powder size analyzer.

*Table 1: Starting powder characteristics*

Powder	Description	Powder sizes (μm)	Purity	Source
Aluminum	Flake	D50 of 51 μm	98% (stabilized 2%)	Merck KGaA
Alumina	Rounded	D50 of 4 μm	99.5%	Merck KGaA
Zinc	Rounded	D50 of 18 μm	96 %	Merck KGaA
Magnesium	Rounded	D50 of 115 μm	98 %	Merck KGaA
Copper	Irregular	D50 of 39 μm	99.5%	Merck KGaA
Iron	Rounded	D50 of 200 μm	99.5%	Merck KGaA
Chrome	Irregular	D50 of 160 μm	99.5%	Merck KGaA
Nickel	Rounded	D50 of 11 μm	99.5%	Merck KGaA

### 2.2 Procedures of Techniques

The PM processing route followed included powder blending, uni-axial die compaction and controlled atmosphere sintering. All powders (it included the addition of 1.5 % stearate acids as die lubrication) were initially blended in a Turbula mixer for twenty minutes. The mixed powders were cold press in a cylindrical steel die Ø 16-mm under 360 MPa pressure using a floating uniaxial die a hand-operated hydraulic cold press to make a compact. The sample has weighed approximately, 3.5 grams. Green compacts sintered in LT furnace and channeled the flow with the pure argon gas. To ensure further purification and eliminate any trace oxygen contamination, argon gas passed through having activated carbon black was inserted inside the gas inlet side of the furnace. The sintering process was carried out at a temperature of 25°C - 650°C for 120 minutes. The heating and cooling rates were set at a constant level be 8°C/min.

The densities of green compacts were determined from the mass and the dimensions of the compacts, while the densities and porosities of the sintered compacts were determined using the Archimedes principle according to the ASTM B 312-09 [12]. After the sintering process accomplished, the compacts were homogenizing treated followed by quenching in cold water immediately after each the step of the homogenizing treatment. To the further optimization, the samples were performed the aging treatment at T6 temper and after that the retrogression and re-aging process followed by the quenching in cold water after each step of the heat treatments respectively, according to the procedure of the T6 temper and RRA process in a schematic presentation as shown in Figure 1.

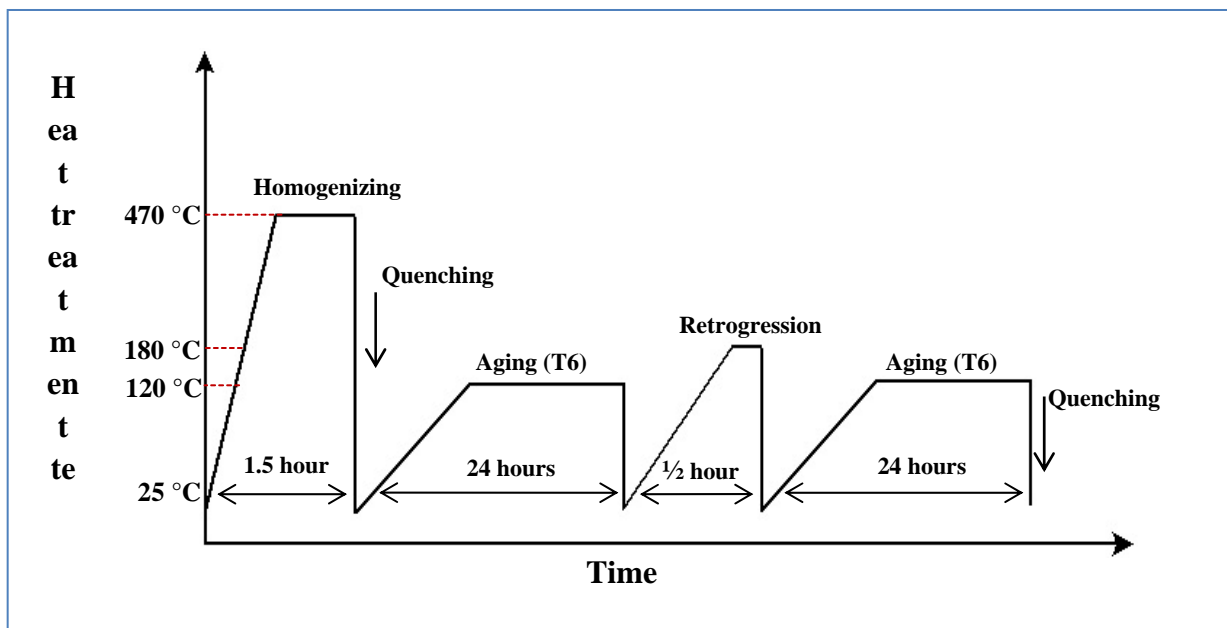


Fig. 1. Schematic present heat treatment cycle of the alloy A after sintering process.

Characterization of the sintered and heat-treated products included the measurement average Vickers Hardness, according to ASTM E92-82, "Mitutoyo DX256 series." Indentation force was set to 20N, and 10 second dwelled time. To ensure cleanliness the surfaces of the compacts were polished prior to HV measurement. Each reading was an average of at least ten separate measurements taken randomly. The highest and the lowest values of the ten readings were disregarded. Microstructures of the alloy A compacts were analyzed by the optical microscopy (OM) using (Olympus PMG3 optical microscope), scanning electron microscopy ((SEM) JEOL JSM-6460LA analytical scanning electron microscope) coupled energy dispersive X-ray spectroscopy (EDS) and X-ray diffraction analysis was ((XRD)SHIMADZU, and X-Ray Diffractometer ) used under the following conditions; scan range: 20°-80°, step size: 0.03, scan rate: 5°/min. The specimens were ground and polished according to ASTM E3-01. They were etched with Keller's reagent.

### 3. Result and discussion

The microstructures of the alloy A composite under investigation is shown in Fig.2 (a) after sintering process, (b) aging at T6 temper and (c) applying RRA process.

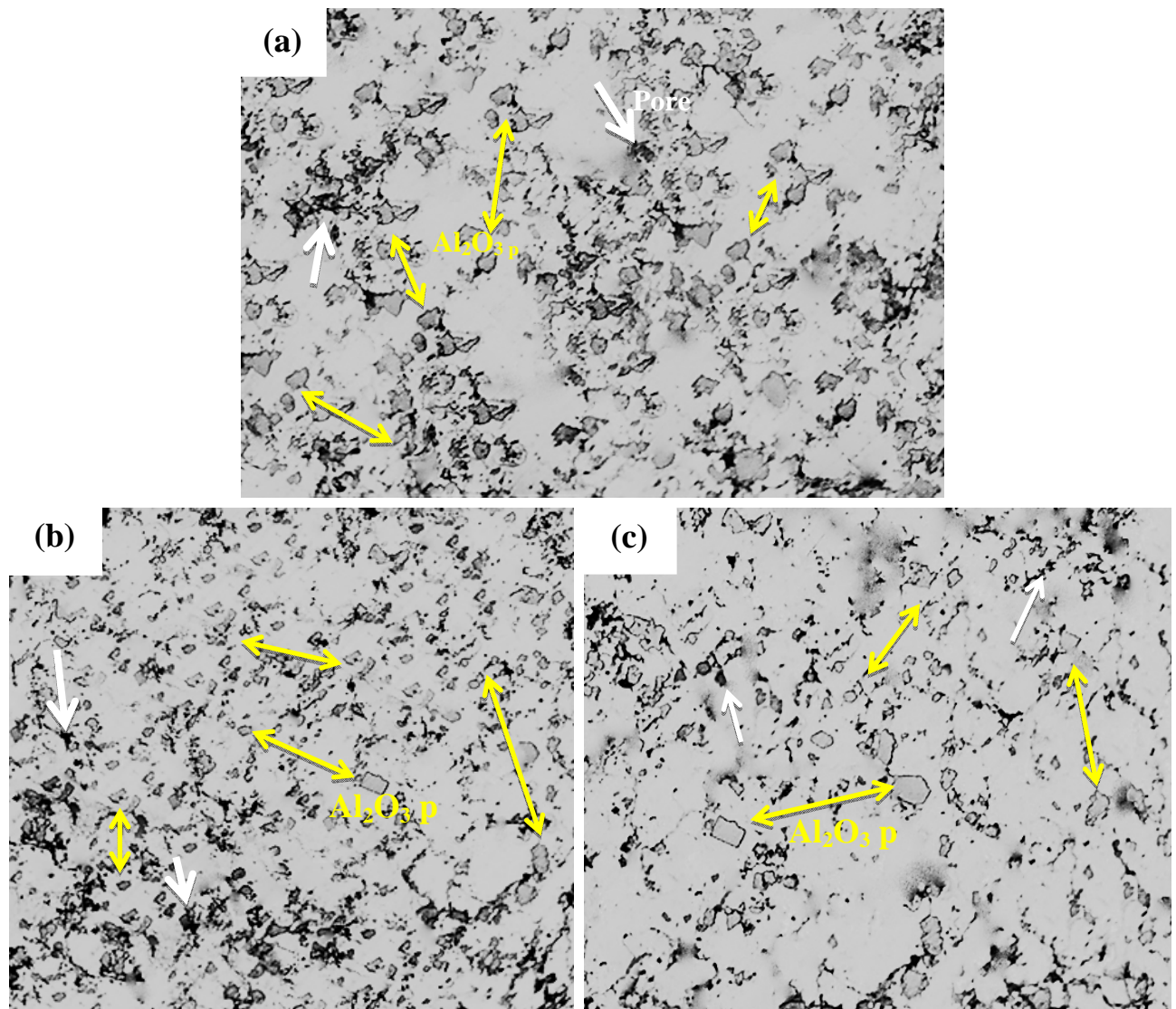


Fig. 2. Optical micrograph of the alloy A: after undergoing (a) sintering process, (b) aging at T6 temper and (c) the retrogression and reaging process.

For the composites of the alloy, A (fabricated using the matrix alloy powder and strengthened with 4  $\mu\text{m}$   $\text{Al}_2\text{O}_3$  particles) a sufficiently uniform reinforcement distribution is observed when the  $\text{Al}_2\text{O}_3$  content is 5 vol. %. In those cases, clusters of the reinforcement particles are formed. Attribute assessed comprising sintered density wherein the average density was determined to be ( $2.5 \text{ g/cm}^3$ ) representing 81.3 % of the full theoretical density ( $3.07 \text{ g/cm}^3$ ). However, the percentages of apparent porosity in the sintered samples were determined to be 3.6 % as indicated in Figs.2 (a), (b) and (c) reveals to the presence of the pores. The reason standing behind that is the vast difference to the melting point of the constituents,  $\text{Al}_2\text{O}_3$  particles are acting as a barrier to the rearrangement, deformation and diffusion of the particles leading to porosity, irrespective to the sintering conditions

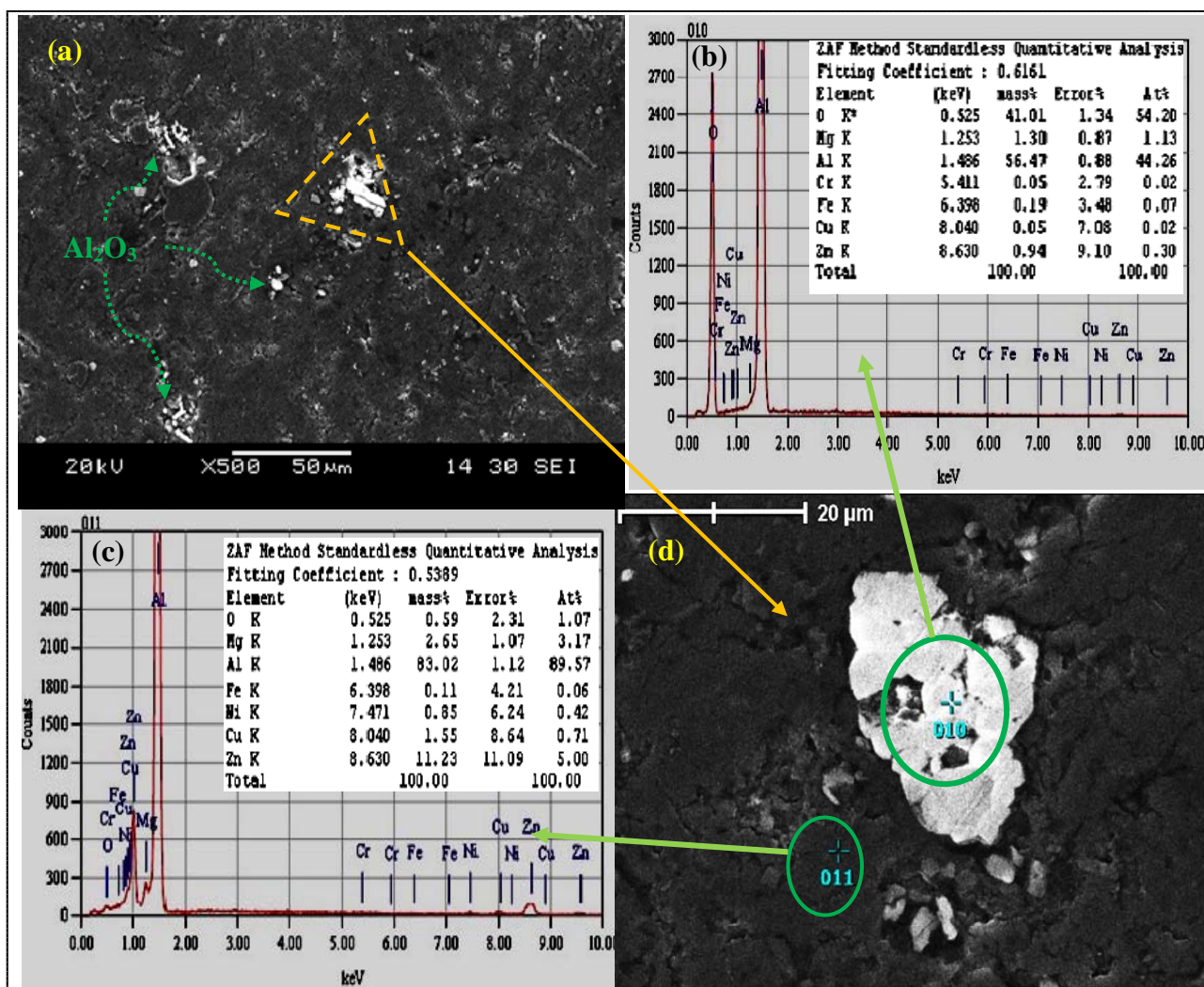


Fig. 3. (a, d) SEM and (b, c) EDS microanalysis of alloy A after applying the sintering process.

To evaluate the microstructure of the as-sintered alloy A composite, the scanning electron micrograph (SEM) represents in Fig. 3a it indicates that the distribution of  $\text{Al}_2\text{O}_3$  particles within the matrix is reasonably uniform with the least agglomeration. Also appearing in Figure 3c high magnification SEM micrographs indicated that interfacial bonding is achieved between the  $\text{Al}_2\text{O}_3$  particulates and aluminium alloy matrix due to small  $\text{Al}_2\text{O}_3$  particles ( $4\ \mu\text{m}$ ) and an advanced sintering at an elevated temperatures. Cheng et al [13-14] also observed this behaviour. The energy-dispersive X-ray spectroscopy (EDS) analysis showed that darker phase is the Al matrix, and the white particles are alumina (Fig. 3b and c) respectively.

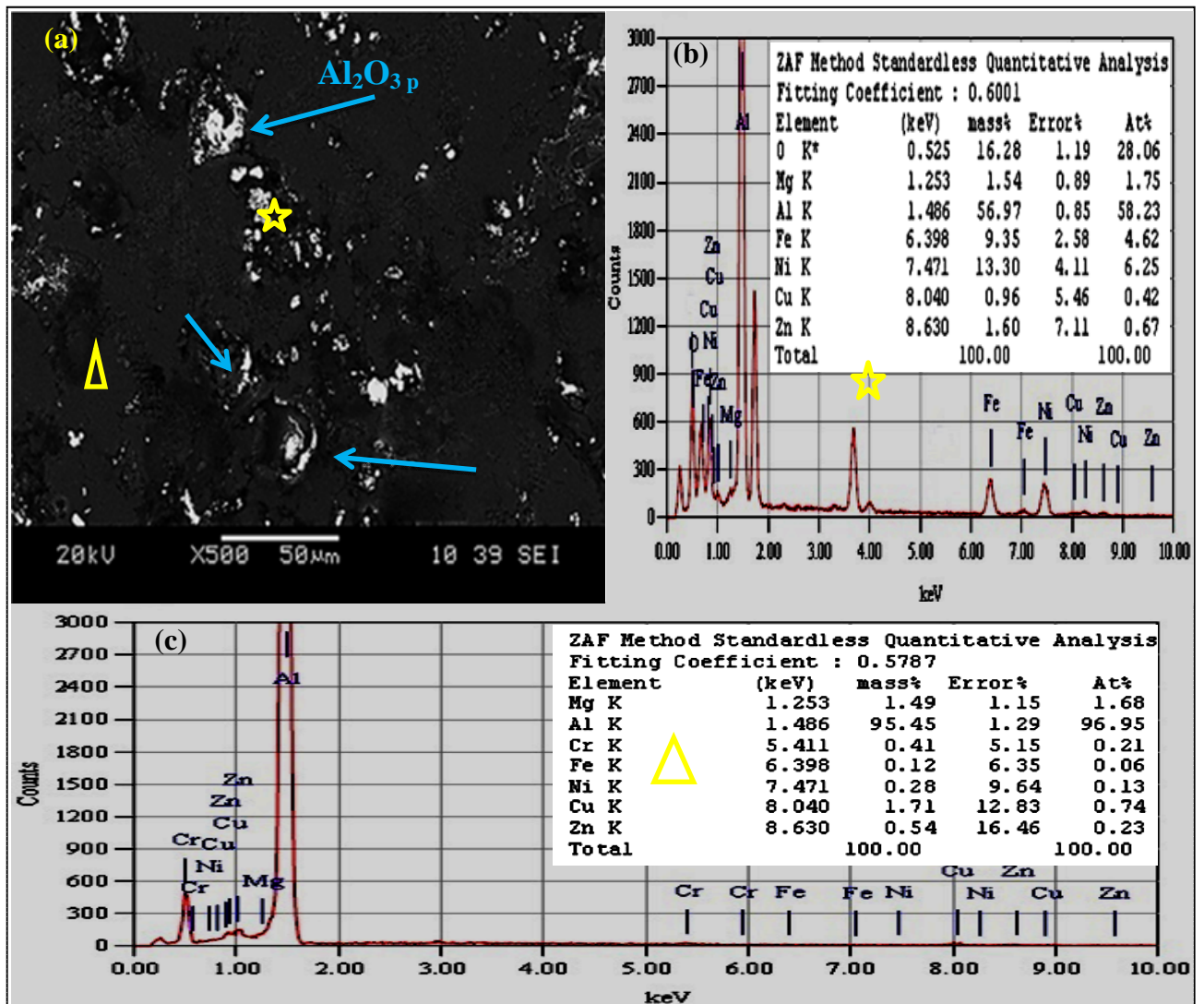


Fig. 4. (a) SEM image and (b, c) EDS microanalysis of the alloy A undergoing, the homogenizing treat and the aging at T6 temper.

After series of the homogenize treatments, subsequently the aging treatment at T6 temper is applied. SEM micrograph in Fig. 4a indicates good distribution of reinforcement's alumina particles within the matrix of alloy A addition the lower agglomeration in the composite. The EDS microanalysis in Fig. 4b revealed that the composite (the labeled region) wherein indicated to the chemical composition of alumina in the matrix, as well as an existence the S-(Al Cu Mg),  $\gamma$ -(Al-Cu-Ni)  $\square$ -(MgZn), and (AlCuFeCr) phases. The EDS analysis shown in Fig. 4c illustrated the chemical composition in the matrix alloy A composite as the labeled region.

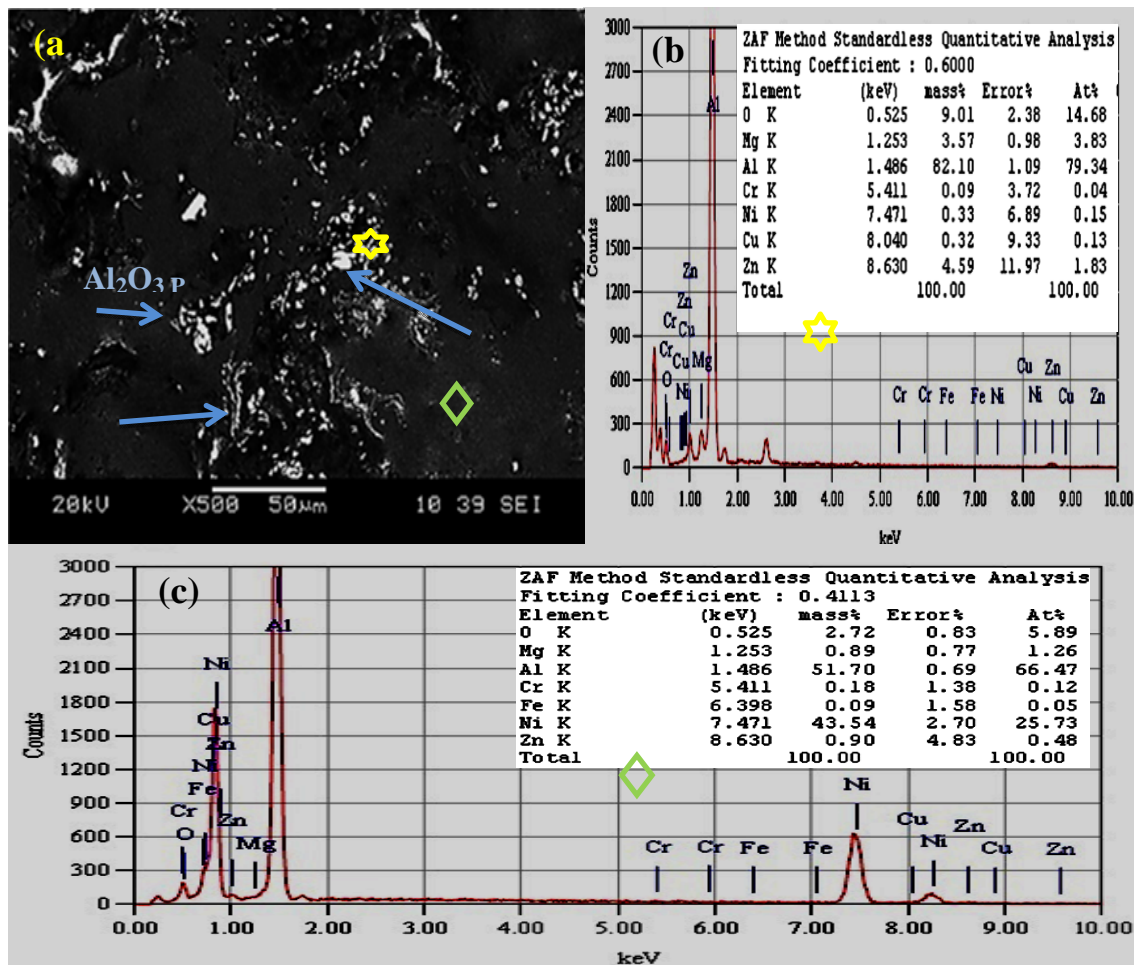


Fig. 5. (a) SEM micrograph and (b) EDS analysis of the alloy A after applying RRA process.

The SEM image shown in Fig. 5a reveals to the micrograph of aluminium alloy composite under applying the RRA treatment. Throughout the EDS analysis of the bright region alloy A composite in Fig. 5b reveals, the stoichiometry of the alumina reinforced in addition to Fig. 5c shown the EDS of the others' phases in the matrix.

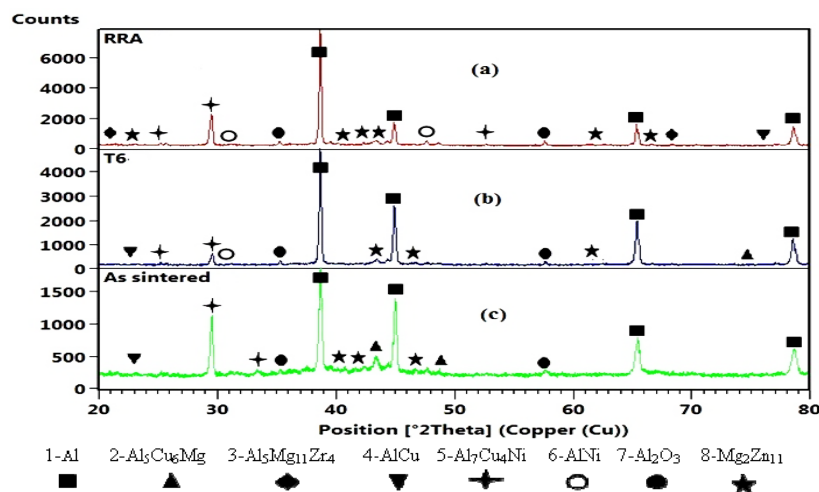


Fig. 6. The XRD plots of the alloy A composite; as sintered, after the impacts of the T6 temper, and the RRA process.

The X-ray diffraction (XRD) in Fig. 6 manifests to the patterns of the alloy A composite after carrying the sintering; the aging at T6 temper, and the RRA process. Fig. 6c refers as sintered alloy A composite sample which fundamentally consisted of alpha-Al, S-Al<sub>5</sub>Cu<sub>6</sub>Mg, AlCu, Mg<sub>2</sub>Zn<sub>11</sub>, Al<sub>2</sub>O<sub>3</sub> and intermetallic compound (i.e. Al<sub>7</sub>Cu<sub>4</sub>Ni). The generally the precipitation hardening sequences for the 7XXX series aluminium alloys are as follows: [15-16]: supersaturated solid solution → coherent stable Guinier–Preston (GP) zones → semi-coherent intermediate η'-phase → Metastable stable η-phase. The primary precipitations in the matrix are the GP zones and η'-phase undergone the aging at 120 °C for 24 hours. As presented in the XRD plots in Fig. 6b; describe alloy A composite sample at the T6 temper whereas reveals to existence AlNi phase intermetallic compound. The XRD results in Figure 6a, exhibited the alloy A matrix after adding (5% of Al<sub>2</sub>O<sub>3</sub>) under the impact on the RRA process; It detects the new creating the Al<sub>5</sub>Mg<sub>11</sub>Zn<sub>4</sub> phase as well as plenty of η'-Mg<sub>2</sub>Zn<sub>11</sub> phase. The precipitation procedure through the matrix of an Al-Zn-Mg-Cu alloy after carrying the RRA process is more detailed by [8, 16-17]. The findings from the XRD analysis were detected to the consistency among the EDS results of the mention former in Figs. 3, 4, 5 (b).

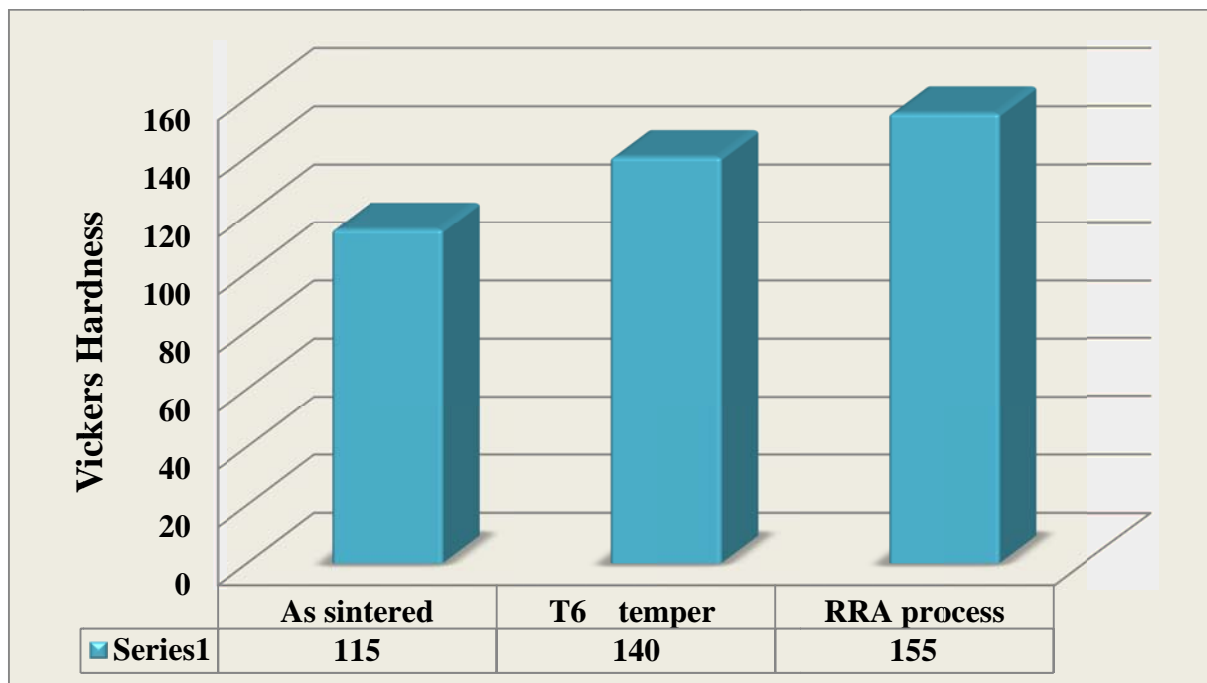


Fig. 7: Vickers's hardness values of the examined alloy A composite sample after different heat treatment conditions.

As it is expected, the hardness measurements verify that the hardness alloy A composite sample's increases from average value of 115 HV (as sintered) to 140 and 155 HV after carrying T6 temper and RRA process, respectively. It can be explained with respect to the distribution of the hard second phase Al<sub>2</sub>O<sub>3</sub> particles within the matrix as well as having intermetallic compounds (i.e. Al<sub>7</sub>Cu<sub>4</sub>Ni, AlNi). Thus, the results show that the hardness of the composite that subjected to the aging at T6 temper, and the RRA is more than the composite as sintered. The findings of this study contrary with the outcomes by Dasgupta [8] showed that an Al-Zn-Mg-Cu matrix composite under the RRA treatment has not given higher hardness.

Improvement of the hardness can be attributed to three phenomena:

1. The precipitation hardening detailed as mentioned a former above.
2. The dispersion strengthening is described that as the addition of alumina particles to aluminum P/M alloy matrix with good distribution and interfacial bonding as well as the existence of Ni-dispersoids particles within the matrix.

The dispersion is attributed to the effects of average alumina particle size of 4 $\mu$ m. Delicate description on Eq. (1) Refer that the distance apart from the reinforcement is reduced while using finer powders as mentioned by [18].

$$\lambda = \frac{4(1-f)r}{3f} \quad (1)$$

Where  $\lambda$  is the distance apart from the reinforcements,  $f$  is the fractional volume of the reinforcement;  $r$  is the radius of the particles (assuming them spherical). When alumina particles act as a barrier during deformation, according to Eq. (2), more energy is required in the movement of dislocations when they encounter a finer hard phase [14, 19-20].

$$\tau_0 = \frac{G b}{\lambda} \quad (2)$$

Where  $\tau_0$  is the stress required for a dislocation to pass reinforcement,  $G$  is the shear modulus of the material and  $b$  is the Berger's vector of the dislocation.

3. Strengthening occurred is due to the coefficient of thermal expansion (CTE) mismatch between the matrix and the reinforcement of alumina, which resulted in a high dislocation density in the matrix.

#### 4. Conclusions

In this research, effectiveness of alumina dispersoids within (7xxx series) aluminum alloy under the retrogression and reaging treatments were investigated. The findings can be summarized as followings:

The relative density of Al-alloy/Al<sub>2</sub>O<sub>3</sub> composite was the high due the containing fine particle sizes.

Regarding of the microstructures and the XRD analysis of an Al-Zn-Mg-Cu-Fe-Cr-Ni alloy/Al<sub>2</sub>O<sub>3</sub> composite samples that appearing a variety of precipitates including the GP zones and  $\eta'$ -Mg<sub>2</sub>Zn<sub>11</sub> phases with existence the intermetallic dispersion as Al<sub>7</sub>Cu<sub>4</sub>Ni and AlNi as well as having Al<sub>2</sub>O<sub>3</sub> hard second phase.

The highest hardness was 155 HV in Aluminum-alloy specimens containing average alumina particle size of 4 $\mu$ m heated at the retrogression and reaging (120 °C for 24 h +180°C for 30 min. + 120 °C for 24 h).

#### Acknowledgements

This work is supported under the University Malaysia Perlis (UniMAP). The authors gratefully acknowledge the outstanding support provided by the technicians of the work shop in the Materials Engineering School, UniMAP.

#### References

- [1] M. Rezayat, A. Akbarzadeh, *Materials and Design*, , **36**, 874 (2012).
- [2] S. Pournaderi, S. Mahdavi, F. Akhlaghi, *Powder Technology* **229**, 276 (2012).
- [3] Majid Hoseinia, Mahmood Meratian, *Journal of Alloys and Compounds* **471**, 378 (2009).
- [4] A.M. Al-Qutub, I.M. Allam, T.W. Qureshi, *Journal of Materials Processing Technology*, **172**, 327 (2006).
- [5] X.P. Zhang, L. Ye, Y.W. Mai, G.F. Quan, W. Wei, *Composites: Part A* **30**, 1415 (1999).
- [6] A.R.I. Khedera, G.S. Marahleh, D.M.K. Al-Jamea, *Jordan Journal of Mechanical and Industrial Engineering*, **5**, 533 (2011).
- [7] L.E.G. Cambronero, E. Sanchez, J.M. Ruiz-Roman, J.M. Ruiz-Prieto, *Journal of Materials Processing Technology*, , **143-144**, 378 (2003).

- [8] Rupa Dasgupta, Humaira Meenai, *Materials Characterization*, **54**, 438 (2005).
- [9] A.D.P. LaDelpha, H. Neubing, D.P. Bishopa, *Materials Science and Engineering, A* **520**, 105 (2009).
- [10] J. Corrochano, M. Lieblich, J. Ibáñez, *Composites Science and Technology*, **69**, 1818 (2009).
- [11] B. Torres, M. Lieblich, J. Ibanez, A. Garcia Escorial, *Scripta Materialia*, **47**, 45 (2002).
- [12] Mateusz L., Jan K., *Acta Polytechnica*, 2012, Vol. 52.
- [13] N.P. Cheng, S.M. Zeng, Z. Y. Liu, *Journal Of Materials Processing Technology* **202**, 27 (2008)
- [14] Mehdi Rahimian, Naser Ehsani, Nader Parvin, Hamid reza B., *Journal of Materials Processing technolog* **209**, 5387 (2009).
- [15] Haider T. Naeem, Kahtan S. Mohammad, *Digest Journal of Nonmaterial and Bio structures*, **8**, 1621 (2013).
- [16] Haider T. Naeem, Kahtan S. Mohammed, *Materials Sciences and Applications*, **4**, 704 (2013).
- [17] Li Guo, Zhang Xin, LI Peng, You Jiang, *Trans. Nonferrous Meta. Soc. China*, **20**, 935 (2010).
- [18] N. Parvin, M. Rahimian, *Acta Physica Polonica A*, 2012, 121, *Proceedings of the International Congress on Advances in Applied Physics and Materials Science, Antalya 2011*.
- [19] Mohsen Hossein-Zadeh, Omid Mirzaee, Peyman Saidi, *Materials and Design*, **54**, 245 (2014).
- [20] Z. Zhang, D.L. Chen, *Scripta Materialia*, **54**, 1321 (2006).